Available online at www.sciencedirect.com
ScienceDirect
International Journal of Heat and Mass Transfer 50 (2007) 625–639
International Journal of HEAT and MASS TRANSFER
www.elsevier.com/locate/ijhmt

Conjugate turbulent natural convection with surface radiation in air filled rectangular enclosures

Anil Kumar Sharma [a], K. Velusamy [a], C. Balaji [b,*], S.P. Venkateshan [b]

[a] *Safety Engineering Division, Safety Group, Indira Gandhi Center for Atomic Research, Department of Atomic Energy, Kalpakkam 603 102, India*
[b] *Heat Transfer and Thermal Power Laboratory, Department of Mechanical Engineering, Indian Institute of Technology Madras, Chennai 600 036, India*

Received 16 March 2006; received in revised form 28 June 2006
Available online 29 September 2006

Abstract

Conjugate turbulent natural convection and surface radiation in rectangular enclosures heated from below and cooled from other walls, typically encountered in Liquid Metal Fast Breeder Reactor (LMFBR) subsystems, have been investigated by a finite volume method for various aspect ratios. The formulation comprises the standard two equation k–ε turbulence model with physical boundary conditions (no wall functions), along with the Boussinesq approximation, for the flow and heat transfer. As far as radiation is concerned, the radiosity – irradiation formulation for a transparent fluid of Prandtl number 0.7 has been employed. The conjugate coupling on the walls has been handled by using a fin type formulation. The Rayleigh number based on the width of the enclosure is varied from 10^8 to 10^{12} and the aspect ratio is varied from 0.5 to 2.0. Detailed results including stream lines, temperature profiles, and convective, radiative and overall Nusselt numbers are presented. A correlation for the mean convection Nusselt number in terms of Rayleigh number and aspect ratio is proposed for design purposes. The influence of the wall emissivity and the external heat transfer coefficient on the heat transfer from the enclosure has also been investigated.
© 2006 Published by Elsevier Ltd.

Keywords: Turbulent natural convection; Surface radiation; Bottom heated enclosure; Transparent media

1. Introduction

Natural convection finds applications in areas like cryogenics, electronics, aeronautics, chemical apparatus, building engineering, solar energy collectors, aerospace systems and nuclear reactor design. In many practical situations, the dimensions of the enclosure are large that the resulting natural convection is turbulent in nature. Natural convection in enclosures is often coupled with surface radiation heat exchange among the walls of the enclosures in transparent fluid media such as air. Surface radiation modifies the wall temperature distribution which, in turn, affects the natural convection bringing in, the interaction effects.

Aydin and Yang [1], numerically studied, laminar natural convection of air in a two dimensional, rectangular enclosure with localized heating from below and symmetrically cooling from the sides for Rayleigh number values 10^3–10^6. They found the flow and temperature fields to be symmetric about the mid width of the enclosure due to the symmetry of the boundary conditions. Hasnaoui et al. [2], numerically, investigated laminar natural convection in an enclosure with localized heating from below and cooled from the top at a constant temperature. The key parameters of the problem were the cavity aspect ratio, position of the heat source and the *Ra* number up to 5×10^6. They found multiple steady state solutions for a given set of governing parameters. Hawkines et al. [3] modeled buoyancy driven laminar natural convection in an enclosure heated from below, cooled from the top with a

* Corresponding author. Tel.: +91 44 22574689; fax: +91 44 22570509.
E-mail address: balaji@iitm.ac.in (C. Balaji).

0017-9310/$ - see front matter © 2006 Published by Elsevier Ltd.
doi:10.1016/j.ijheatmasstransfer.2006.07.022

Nomenclature

AR	aspect ratio of the enclosure, H/W
B	radiosity, W/m^2
C_p	isobaric specific heat of the fluid, kJ/kg K
C_μ, $C_{\varepsilon 1}$, $C_{\varepsilon 2}$, $C_{\varepsilon 3}$	constants in the turbulence model
F_{i-j}	view factor from element i to j
g	acceleration due to gravity, 9.81 m/s^2
G	irradiation, W/m^2
h	heat transfer coefficient, W/m^2 K
H	height of the enclosure, m
k_{eff}	effective thermal conductivity, W/m K
k_{f}	thermal conductivity of fluid, W/m K
k_{w}	thermal conductivity of enclosure walls, W/m K
k	turbulent kinetic energy, m^2/s^2
L	characteristic length of the enclosure, m
Nu_{C}	mean convection Nusselt number, $q_{\text{C}}\, L/k_{\text{f}}\Delta T$
Nu_{R}	mean radiation Nusselt number, $q_{\text{R}}\, L/k_{\text{f}}\Delta T$
Nu_{T}	total Nusselt number, $Nu_{\text{C}} + Nu_{\text{R}}$
p	pressure, Pa
Pr	Prandtl number, ν/α
q_{C}	convective heat flux, W/m^2
q_{R}	radiative heat flux, W/m^2
Ra	Rayleigh number, $g\beta\Delta TL^3/\nu\alpha$
T	temperature, K
ΔT	temperature difference, K
t_{w}	thickness of enclosure wall, m
u, v	horizontal and vertical velocity components, m/s
W	width of the enclosure, m
x, y	horizontal and vertical coordinates, m

Greek symbols

α	thermal diffusivity of fluid, m^2/s
β	isobaric cubical expansion coefficient of fluid, K^{-1}
ε	dissipation rate of k, m^2/s^3, also hemispherical total emissivity of the enclosure surfaces
ψ	stream function, m^2/s
μ	dynamic viscosity of the fluid, Ns/m^2
μ_{t}	turbulent viscosity, Ns/m^2
ν	kinematic viscosity of fluid, m^2/s
ρ	density of the fluid, kg/m^3
σ	Stefan–Boltzmann constant, 5.67×10^{-8} W/m^2 K^4
σ_{k}, σ_{T}, σ_ε	turbulent Prandtl numbers of k, T and ε

Subscripts

a	air
b	bottom wall
c	cold wall
ext	external
h	hot wall
max	maximum value
R	values related to radiation
t	turbulent
T	total contribution of convection and radiation

horizontal partition and having an opening between the two chambers. Based on their numerical study, they proposed a correlation for the average Nusselt number for various values of the compartment aspect ratio. All these studies did not take into account of radiation heat transfer. Lacoa and Campo [4] studied the interaction of laminar natural convection and thermal radiation in a square cavity with differentially heated vertical walls. They found that the interaction effects are significant for lower values of *Ra*, while the converse is true for higher values of *Ra*. They also found that the radiation Nusselt number has a power law relation with the Rayleigh number.

Balaji and Venkateshan [5] carried out a numerical investigation of free convection coupled with surface radiation in a rectangular enclosure. They concluded that calculations that include radiation are more realistic, since it is impossible in practice to have a surface with zero emissivity. Marcelo et al. [6] investigated natural convection in rectangular enclosures heated from below and symmetrically cooled from the sides using the stream function-vorticity formulation for Rayleigh numbers from 10^3 to 10^7 and aspect ratios from 1 to 9. The flow structure was found to form a counter clockwise cell for all the cases studied, except for a small secondary cell in some cases for a uniform temperature at the cavity floor. They also reported the influence of *Ra*, *Pr* and AR on the motion and on the energy transport. November and Nansteel [7] studied natural convection in rectangular enclosures heated from below and cooled along one side. Asymptotic expressions were determined for the temperature and the heat transfer rate near the flux singularity on the enclosure floor. An experimental and numerical study of free convective heat transfer in square enclosures heated from below was carried out by Calcagni et al. [8] for values of *Ra* in the range of 10^3–10^6. The local Nusselt number was evaluated on the heat source surface. The variation of the local Nusselt number on the heat source and the average Nusselt number were presented.

Markatos and Pericleous [9] analyzed buoyancy driven laminar and turbulent flow and heat transfer in a square cavity with differentially heated side walls. In this study a series of Rayleigh numbers (*Ra*), ranging from 10^3 to 10^{16} was analyzed and correlations for the maximum, minimum and average Nusselt numbers were presented. The correlations were compared with experimental data. Hen-

kes [10], studied turbulent natural convection in enclosures filled with air and water, using the standard k–ε model and found the transition Rayleigh number to be very close to the stability limit of steady state laminar solution. The standard k–ε model of turbulence permits to find $Ra_{trans} \approx 10^8$ for air and $Ra \approx 10^{10}$ for water. Henkes and Hoogendoorn [11] carried out a comparison of numerical results obtained by 10 groups of researchers for a standard test case, which was defined for turbulent natural convection flow in an enclosure and presented a standard solution for turbulent natural convection in square cavities. Bilgen [12] studied laminar and turbulent natural convection in an enclosure with partial partitions. The two dimensional conservation equations of mass, momentum and energy, with the Boussinesq approximation, were solved using the SIMPLER method. The Rayleigh number was varied from 10^4 to 10^{11}. A correlation for the heat transfer rate for $10^9 \leqslant Ra \leqslant 10^{11}$ was derived for practical design problems with the partition hanging from the ceiling and extended from the floor. The partitioned walls were found to influence the heat transfer and flow distribution significantly.

The above review of literature indicates that laminar natural convection in bottom heated enclosures has been studied for pure natural convection condition as well as its interaction with surface radiation. Literature on turbulent natural convection is abundant for the traditional case of differentially heated vertical walls with adiabatic horizontal walls. However, literature on turbulent natural convection for bottom heated enclosures appears to scarce, despite its practical relevance in the fields of building design and research and design of LMFBR sub-systems. The presence of other modes of heat transfer (i.e., radiation and conduction in the walls) significantly influences the generally weak natural convection. Hence, it is essential to have a comprehensive investigation of the interaction effects between turbulent natural convection and other modes of heat transfer. In the present study, we have analyzed the interaction effects between surface radiation and turbulent natural convection in enclosures heated from below. The influence of the wall emissivity and the external heat transfer coefficient on the heat transfer from the enclosure is also investigated in detail. The modeling is made more realistic by including conjugate convection in the wall, mimicking a LMFBR subsystem, for example.

2. Physical and numerical modeling

2.1. Physical model and assumptions

The schematic of the two dimensional enclosure of height H and width W (in this study, $W = L$, the characteristic length of the enclosure) is depicted in Fig. 1a. The walls of the enclosure are of finite thickness t_w and finite thermal conductivity k_w. The floor of the enclosure is maintained at a constant temperature, T_h, the external surfaces of which are exposed to ambient temperature at T_c with a heat transfer coefficient of h_{ext} and the internal surfaces of the enclosure walls are exposed to turbulent natural convection of air and surface radiation heat exchange. Air is assumed to be incompressible and radiatively non-participating, with the change in density being incorporated through the Boussinesq approximation.

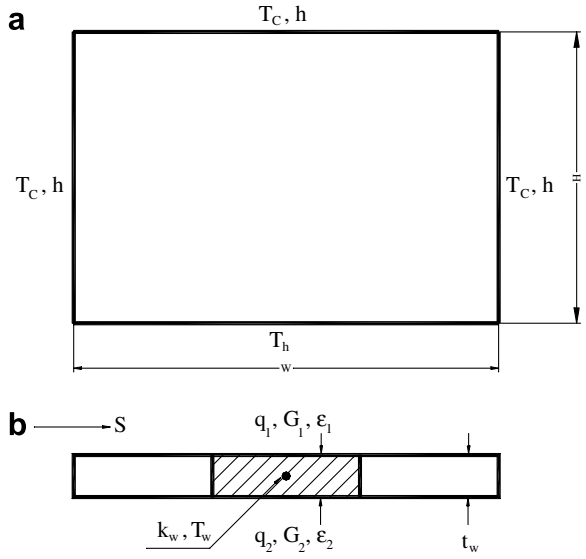

Fig. 1. Physical model and heat balance for elemental wall.

2.2. Governing equations

The turbulent flow considered is described mathematically by the Reynolds averaged Navier Stokes (RANS) equations, including the time averaged energy equation for the mean temperature field that drives the flow by the buoyancy force. The RANS equations for mass, momentum and energy conservation reduce to:

$$\frac{\partial}{\partial x}(\rho u) + \frac{\partial}{\partial y}(\rho v) = 0 \tag{1}$$

$$\frac{\partial}{\partial x}(\rho uu) + \frac{\partial}{\partial y}(\rho vu) = -\frac{\partial p}{\partial x} + \frac{\partial}{\partial x}\left[2\mu_{\text{eff}}\frac{\partial u}{\partial x}\right] + \frac{\partial}{\partial y}\left[\mu_{\text{eff}}\left(\frac{\partial u}{\partial y} + \frac{\partial v}{\partial x}\right)\right] \tag{2}$$

$$\frac{\partial}{\partial x}(\rho uv) + \frac{\partial}{\partial y}(\rho vv) = -\frac{\partial p}{\partial y} + \frac{\partial}{\partial x}\left[\mu_{\text{eff}}\left(\frac{\partial v}{\partial x} + \frac{\partial u}{\partial y}\right)\right] + \frac{\partial}{\partial y}\left[2\mu_{\text{eff}}\frac{\partial v}{\partial y}\right] + \rho\beta g(T - T_0) \tag{3}$$

$$\frac{\partial}{\partial x}(\rho uC_pT) + \frac{\partial}{\partial y}(\rho vC_pT) = \frac{\partial}{\partial x}\left[k_{\text{eff}}\frac{\partial T}{\partial x}\right] + \frac{\partial}{\partial y}\left[k_{\text{eff}}\frac{\partial T}{\partial y}\right] \tag{4}$$

$$\frac{\partial}{\partial x}(\rho uk) + \frac{\partial}{\partial y}(\rho vk) = \frac{\partial}{\partial x}\left[\left(\mu + \frac{\mu_t}{\sigma_k}\right)\frac{\partial k}{\partial x}\right] + \frac{\partial}{\partial y}\left[\left(\mu + \frac{\mu_t}{\sigma_k}\right)\right]\frac{\partial k}{\partial y} + p_k + G_k - \rho\varepsilon \tag{5}$$

$$\frac{\partial}{\partial x}(\rho u\varepsilon) + \frac{\partial}{\partial y}(\rho v\varepsilon) = \frac{\partial}{\partial x}\left[\left(\mu + \frac{\mu_t}{\sigma_\varepsilon}\right)\frac{\partial \varepsilon}{\partial x}\right] + \frac{\partial}{\partial y}\left[\left(\mu + \frac{\mu_t}{\sigma_\varepsilon}\right)\right]\frac{\partial \varepsilon}{\partial y} + [C_{\varepsilon 1}(P_k + C_{\varepsilon 3}G_k) - C_{\varepsilon 2}\varepsilon]\frac{\varepsilon}{k} \tag{6}$$

where

$$P_k = \mu_t\left[2\left(\frac{\partial u}{\partial x}\right)^2 + 2\left(\frac{\partial v}{\partial y}\right)^2 + \left(\frac{\partial u}{\partial y}+\frac{\partial v}{\partial x}\right)^2\right];$$

$$G_k = -\frac{\mu_t}{\sigma_T} g\beta\frac{\partial T}{\partial y}; \quad \mu_{eff} = \mu + \mu_t;$$

$$\mu_t = C_\mu\frac{\rho k^2}{\varepsilon} \quad \text{and} \quad k_{eff} = k_f + \frac{\mu_t c_p}{\sigma_T}.$$

For the k–ε turbulence model the following constants are used:

$C_\mu = 0.09; C_{\varepsilon 1} = 1.44; C_{\varepsilon 2} = 1.92; \sigma_T = 1.0; \sigma_k = 1.0$ and $\sigma_\varepsilon = 1.3$

In the present model, $C_{\varepsilon 3}$ is taken as tanh (v/u), as suggested by Henkes [10]. No wall functions are used and sufficiently fine grids are employed close to the walls, to enable integration up to the walls.

The bottom wall is isothermal at T_h while the temperature variation along the other three walls can be determined including the effect of surface radiation, turbulent natural convection of air and heat conduction in the wall, considered in conjugation. The walls are sufficiently thin so that the temperature variation in the thickness direction is negligible. Thus, the generalized energy balance equation over an elemental wall segment by considering the wall to be a fin (one-dimensional approximation) having diffuse gray surfaces, shown in Fig. 1b, can be expressed as

$$k_w t_w\frac{\partial^2 T_w}{\partial s^2} + q_1 + q_2 + \varepsilon_1 G_1 + \varepsilon_2 G_2 = (\varepsilon_1+\varepsilon_2)\sigma T_w^4, \qquad (7)$$

where k_w, t_w and T_w are the thermal conductivity, thickness and temperature of the wall, s is the length measured along wall and ε is the hemispherical emissivity of the wall surface. G is the irradiation falling on the wall surface and subscripts 1 and 2 refer to conditions on the external and internal surfaces of the wall. The convective heat flux, q_1, is evaluated from the ambient fluid temperature, ambient heat transfer coefficient and T_w. The convective heat flux, q_2, is evaluated from $q_2 = k_f(T - T_w)/\Delta n$, where k_f and T are the thermal conductivity and local temperature of fluid in the enclosure, adjacent to the wall, respectively, and Δn is the normal distance of the first fluid node from the wall surface. The irradiation is related to radiosity (B), through the relation

$$B_i = \varepsilon_i\sigma T_{wi}^4 + (1-\varepsilon_i)G_i, \qquad (8)$$

where subscript i is the index of the elemental segments forming the enclosure. Substituting for G in terms of B and using the inverse relationship, we get

$$G_i = \sum_{j=1}^{N} B_j F_{i-j} \text{ and } \sum\left[\frac{\delta_{ij} - (1-\varepsilon_i)F_{i-j}}{\varepsilon_i}\right]B_j = \sigma T_i^4, \qquad (9)$$

where F_{i-j} is the shape factor from segment i to segment j, δ_{ij} is the Kronecker delta and N is the total number of radiating segments. Eq. (7) forms a set of tri-diagonal algebraic equations on discretisation, for the nodal temperatures of each wall, which need to be solved in conjunction with Eqs. (8) and (9). It is also connected to Eqs. (1)–(6), through the wall temperatures T_w. Thus, the interfacial requirements are the continuity of temperature and heat flux between adjacent media.

The wall under consideration for a typical application like LMFBR subsystems is thin and so $t_w = 10$ mm. The wall material is assumed to be stainless steel with $k_w = 20$ W/m K. Even with the highest assumed value of

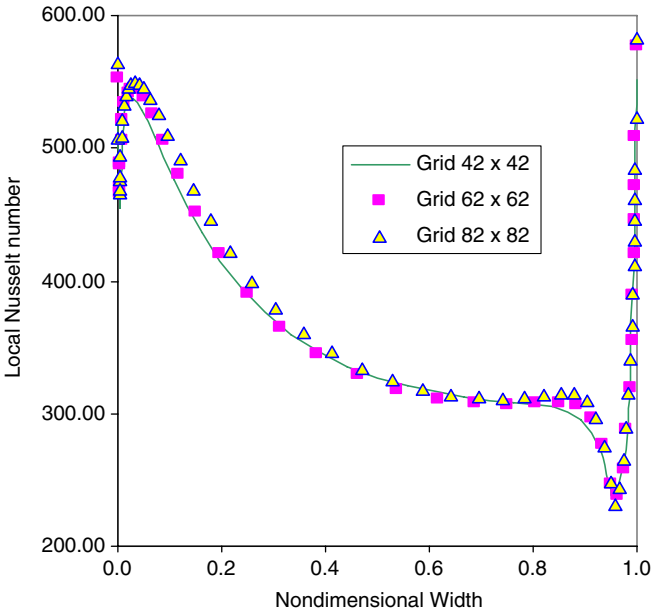

Fig. 2. Variation of the local Nusselt number on the bottom wall for various grid sizes.

Table 1
Comparison of the predicted mean Nusselt number on the vertical walls of the enclosure and non dimensional maximum velocity with benchmark results

Rayleigh number	Present study		De Vahl Davis [15]		% Deviation	
	Nu	V_{max}	Nu	V_{max}	Nu	V_{max}
10^3	1.127	3.661	1.118	3.697	0.805	0.97
10^4	2.258	19.417	2.243	19.617	0.66	1.0
10^5	4.499	68.86	4.519	68.59	0.44	0.39

Table 2
Comparison of present predictions of average Nusselt number with published solutions for turbulent natural convection

Rayleigh number	Average Nusselt number				
	Present study	Markatos and Pericleous [9]	Henkes [10]	Dixit and Babu [16]	Elsherbiny et al. [19] (Experimental)
10^8	30.97	32.04	–	30.50	28.78
10^9	58.33	74.96	58.51	57.35	62.0
10^{10}	130.77	159.89	137.5	103.66	133.57
10^{11}	325.9	341.05	320.96	–	287.78
10^{12}	673.80	727.47	744.68	–	620.0

the external heat transfer coefficient (h_{ext}) of 40 W/m^2 K, the Biot number, $Bi = h_{ext}t_w/k_w$ is 0.02 and so the one dimensional fin model for the solid walls is justified.

2.3. Boundary conditions

Eqs. (1)–(6) are subjected to the boundary conditions, $u = 0$, $v = 0$, $k = 0$, $\varepsilon = \infty$ (numerical infinity) and $T = T_w$ on the solid walls. For the limiting case of infinite heat transfer coefficient on the external surface the left, right and top walls are isothermal at T_c. The floor or the bottom wall is subjected to an isothermal condition of T_h for all the cases. For the cases where interaction of radiation with turbulent natural convection is investigated, the outer surfaces of the left, right and the top walls are subjected to an external convective heat transfer coefficient

Table 3
Comparison of the Nusselt number and non dimensional maximum velocity

Rayleigh number	Present study		Hawkines et al. [3]		% Deviation	
	Nu	V_{max}	Nu	V_{max}	Nu	V_{max}
10^4	2.16	21.67	2.17	22	0.5	1.5
10^5	3.98	99.4	3.93	104	1.2	4.4
10^6	7.22	385	7.25	395	0.4	2.5

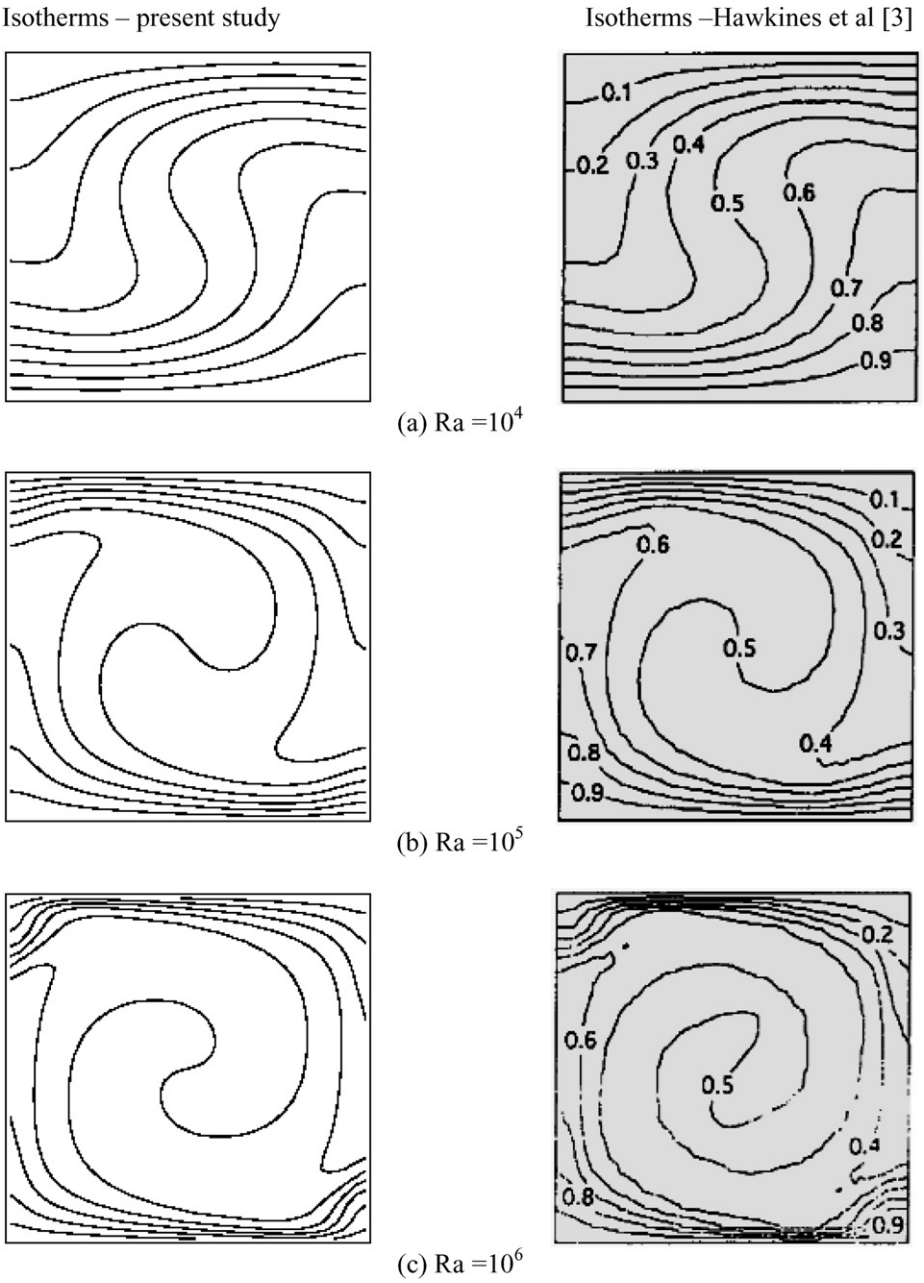

Fig. 3. Comparison of temperature contours with the numerical results of Hawkines et al. [3].

of 5 W/m^2 K (unless otherwise stated), while the bottom wall is kept isothermal at T_h.

2.4. Solution methodology

For the numerical solution of these equations, the primitive variable approach, wherein the velocity components and the pressure are independent variables, is adopted. The spatial derivatives in the equations are discretized using the finite-volume method. The enclosure is filled with a non-uniform rectangular staggered grid, with a very fine spacing near the walls, for accurately resolving the steep gradients in the thin buoyancy-driven boundary layers. A grid distribution scheme, suggested by Henkes [10], is used to enable fine grids near the wall and coarse grids away from the walls which results in very low values for y^+ ($y^+ = y\ u_\tau/v$, u_τ is the frictional velocity given by $\sqrt{\tau_w/\rho}$ where τ_w is the wall shear stress). Typically, for turbulent natural convection flows, the viscous sublayer extends up to $y^+ \approx 1$. These low values for y^+ (<0.35) imply that the present calculations are able to resolve even the viscous sublayer. The SIMPLE algorithm proposed by Patankar

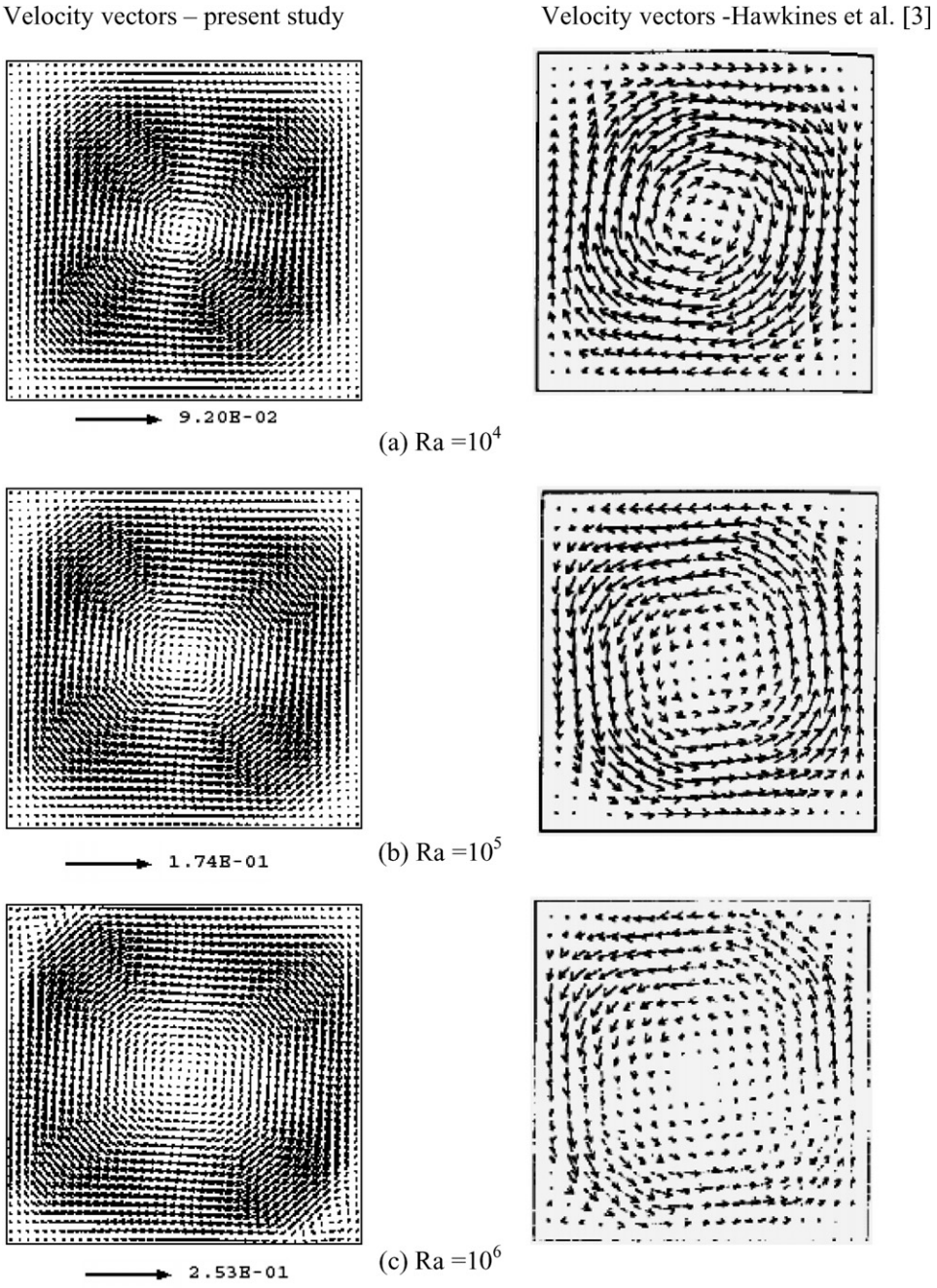

Fig. 4. Comparison of velocity vectors with the numerical results of Hawkines et al. [3].

and Spalding [13], is used to resolve the pressure–velocity coupling. The discretised equations are solved using the line by line Thomas algorithm with two directional sweeps.

As regards radiation, the view factors were evaluated using the Hottel's crossed string method [14]. The radiosities of the elemental wall surfaces are expressed as a function of elemental wall surface temperature, emissivity and the shape factors. The radiosity (B_i) and temperature (T_i) are connected by a matrix of the type

$$[A_{i,j}]\ \{B_i\} = \{\sigma T_i^4\} \tag{10}$$

The inverse of the matrix $[A_{i,j}]$ is determined (only once) by the Gauss elimination method. The coefficients of $[A]$ are constants and depend only on the emissivity and the shape factors have no dependence on the temperatures.

In order to determine convergence criteria of the iterative solutions, the absolute sum of the errors in the discretisation equations of all the points for any variable Φ, is taken as the error $= \sum_{i=1}^{N} |a_p\phi_p - \sum a_{nb}\phi_{nb} - b|_i$ and is normalized with respect to a reference value. The reference value for the continuity equation is the recirculation mass flow rate, i.e., $\int_0^{w/2} \rho v_{y=H/2} dx$, where w is the width of the enclosure and v is the vertical velocity at mid height. For the momentum equation, it is the recirculation flow rate multiplied by maximum velocity in the domain. For the energy equation it is the mass flow rate multiplied by the specific heat and temperature difference. Similarly for the k and ε equations, it is the mass flow rate multiplied by maximum values of k and ε inside the domain. The normalized error should be less than 10^{-3} for all the variables. At the same time, important parameters like Nu_C, Nu_R, heat transfer rates for various walls surfaces and velocities are monitored all through the iteration along with heat imbalance. At convergence, the heat imbalance criterion is set as 0.1% and the variables at the monitoring locations simultaneously satisfy the normalized error criteria, discussed earlier.

3. Grid independence study and validation

The independence of the solution with respect to the grid size is studied for a Rayleigh number of 10^{10} and an aspect ratio (AR) of 1.0. Three different grid sizes of 42×42, 62×62 and 82×82 are used for the grid independence study. The smallest grid size in the case of 42×42 grids is $\sim 5 \times 10^{-5}$ and the same in the case of 82×82 grids is $\sim 2 \times 10^{-5}$. Fig. 2 shows the variation of the local Nusselt number on the bottom wall of the enclosure for various grid sizes. It is clear that the variation of the local Nusselt number on the bottom wall for various grid sizes is nearly identical. The maximum difference in terms of the overall Nusselt number for the various grids is less than 0.85%, indicating that a 42×42 grid is sufficient to model accurately the heat transfer and fluid flow inside the enclosure. Hence, a grid size 42×42 has been used in all the subsequent computations for $Ra \leqslant 10^{10}$. For $Ra > 10^{10}$, a 180×180 grid leading to grid independent solutions is used.

The code is validated first for the limiting case of laminar natural convection with the bench mark solution of De Vahl Davis [15] with a uniform grid of 42×42. The comparison is performed for the case of a square compartment with differentially heated vertical walls and adiabatic horizontal walls, for $Ra = 10^3$, 10^4 and 10^5, in terms of the average Nusselt number and maximum velocity in the enclosure. The results obtained with the present code along with the percentage deviation with respect to the results given in [15] are given in Table 1. It can be seen that the agreement is very good, with a maximum deviation of only 1% in the mean Nusselt number and the vertical velocity.

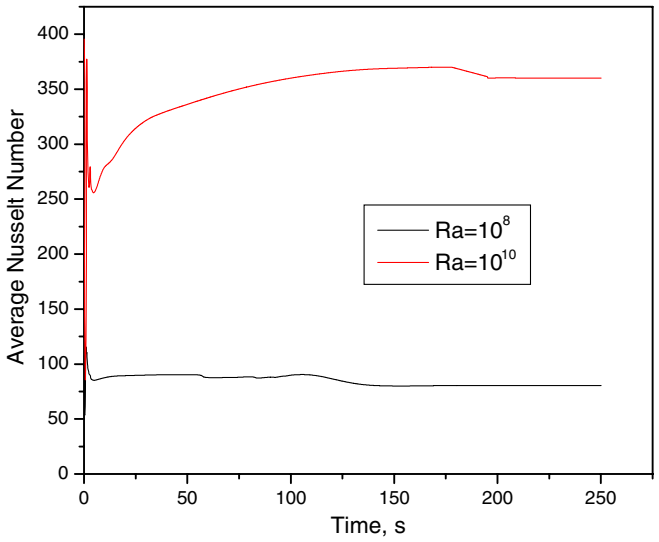

Fig. 5. Variation of the average Nusselt number on the bottom wall with time for AR = 1.0.

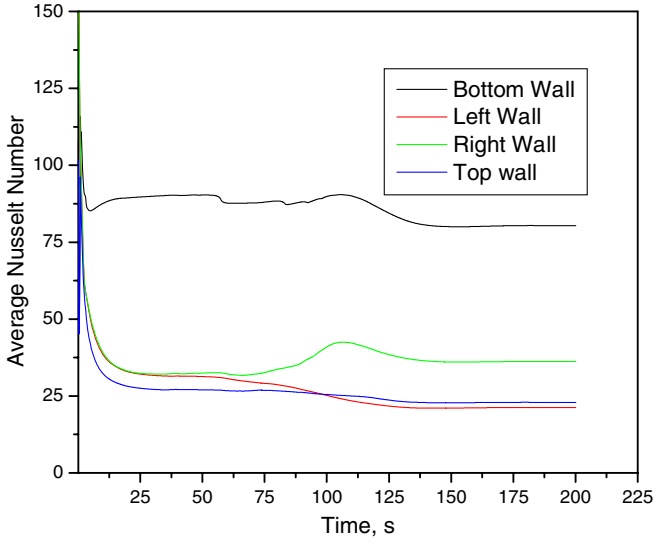

Fig. 6. Variation of the average Nusselt number on all four walls of the enclosure with time for $Ra = 10^8$ and AR = 1.0.

To validate the numerical code for turbulent simulations, natural convection of air in a square compartment has been considered for Rayleigh numbers in the range from 10^8 to 10^{12} and the results obtained are compared with those of Markatos and Pericleous [9] as well as the work reported by Henkes [10]. Table 2 gives a comparison of these results in the form of average Nusselt number. The maximum deviation at the high *Ra* number is, respectively, 9.5% and 7.4% when compared with numerical results of Henkes [10] and Markatos and Pericleous [9]. Also presented in the same Table are the very recent results of Dixit and Babu [16], who used a thermal lattice Boltzmann method, based on the BGK model to simulate high Rayleigh number natural convection in a square enclosure. In addition to the above comparisons, the results of the experimental correlation proposed by Elsherbiny et al. [19], for large aspect ratio enclosures with air as the medium, for *Ra* number up to 10^7 are highlighted in the table. It can be seen that the predictions of the present study are closer to the experimental data than the other numerical results.

Similarly, the problem of laminar natural convection in a square enclosure with isothermal top and bottom walls and adiabatic side walls was solved using the code. The bottom wall is hot and the top is cold. The predicted results

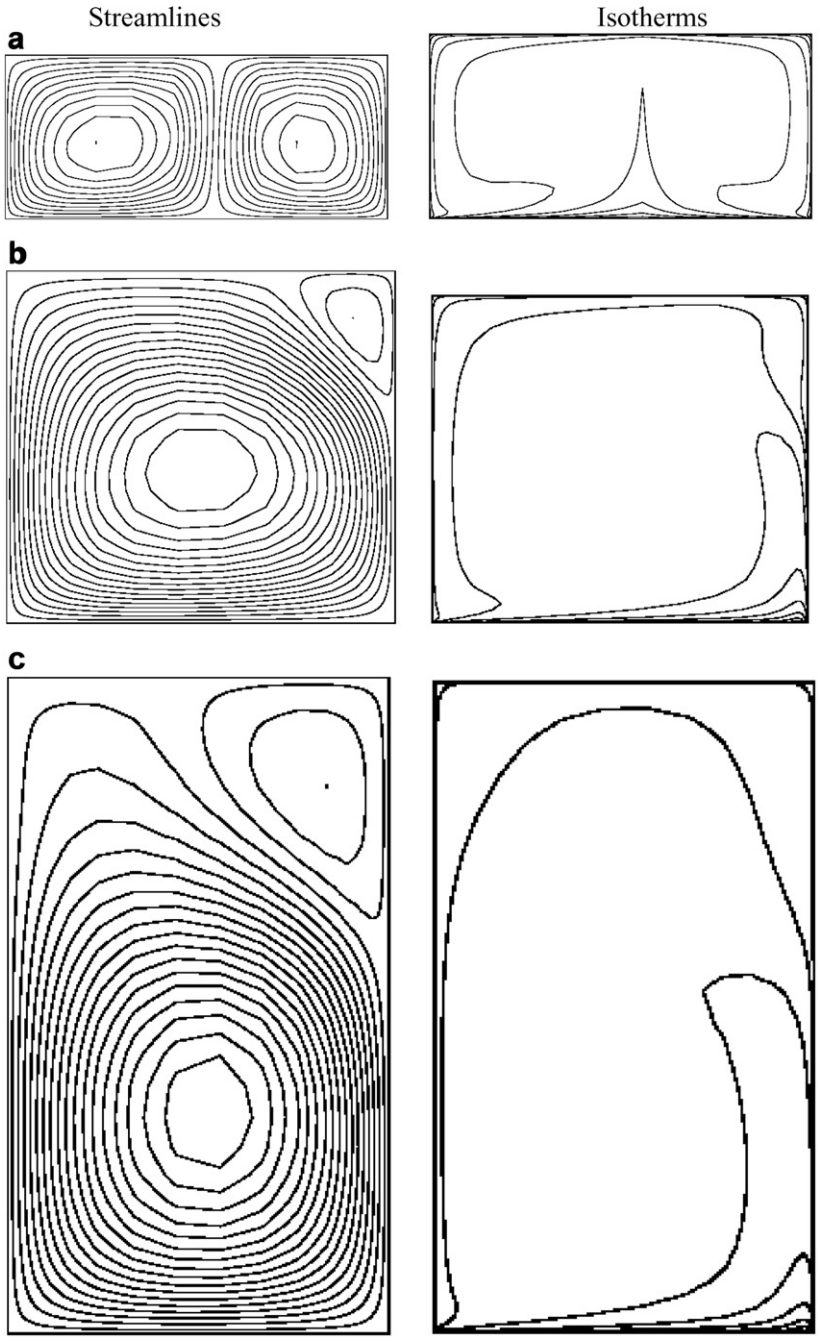

Fig. 7. Streamlines and isotherms: (a) AR = 0.5, $\psi_{max} = 0.328$; (b) AR = 1.0, $\psi_{max} = 0.799$ and (c) AR = 2.0, $\psi_{max} = 1.08$ for $Ra = 10^{12}$.

of mean Nusselt number and non dimensional maximum vertical velocity are compared with the numerical results of Hawkines et al. [3] in Table 3. Maximum deviations of 1.2% and 4.4%, respectively, in the Nusselt number and the non-dimensional maximum velocity are observed. Figs. 3 and 4 show the temperature contours and velocity vectors, respectively (for Ra 10^4, 10^5 and 10^6). It is interesting to observe that although the boundary conditions are symmetric about $x/W = 0.5$, the resulting natural convection is not symmetric. Typically, a unicell flow pattern is observed with secondary vortices around the corners. The flow distribution is anti-symmetric about the diagonal connecting the lower left corner and the upper right corner. It is clear that the results obtained from present code compare well with the published results.

The problem under investigation corresponds to a situation of unstable stratification with the bottom wall heated. For laminar natural convection in enclosures with bottom wall heating, researchers [2,17] have observed oscillatory convection. Hence, it is essential to verify whether such oscillatory convection prevails for present enclosures. Towards this the governing Eqs. (1)–(6) are solved in their transient form for some representative cases. The evolution of average Nusselt number on the hot wall as a function of time is presented in Fig. 5 for Ra 10^8 and 10^{10}. It can be seen that the Nusselt numbers reach non-oscillatory stable steady value after about 200 s. Also, these stable values of Nusselt number are exactly same as those predicted by solving the steady state form of governing equations, which are discussed in the subsequent section. The transient evolution of Nusselt numbers on the four walls of the enclosure for $Ra = 10^8$ is depicted in Fig. 6. It can be seen that that the individual Nusselt numbers on all the four walls attain, the stable steady value, which are again equal to those obtained from steady state solution. Thus these exercises demonstrate the adequacy of the steady state formulation and the resulting solution for the problem of turbulent natural convection in an enclosure whose bottom wall is heated.

These validation studies demonstrate that the code developed is capable of predicting natural convection in enclosure for stable and unstable stratification, both in the laminar and turbulent regimes.

4. Results and discussion

To understand the flow and heat transfer characteristics for turbulent natural convection in the enclosure, depicted in Fig. 1, four major influencing parameters are considered and the results obtained are given below in separate subsections. In the first subsection 4.1, the walls of the enclosure are assumed to be very thin and the external heat transfer coefficient is infinite. This leads to the bottom wall being isothermal at T_h and the other three walls being isothermal at temperature T_c. Since the walls are at isothermal condition, surface radiation has no role in modifying the wall temperatures. So there is no interaction between natural convection and surface radiation in the transparent medium. In the second subsection 4.2, the surface radiation interaction with turbulent natural convection is considered for $10^8 \leqslant Ra \leqslant 10^{12}$. The third subsection 4.3 details the influence of the emissivity on the overall heat transfer and in the last subsection 4.4, the effect of the wall heat transfer coefficient is studied, in detail.

4.1. Flow field and heat transfer in the enclosure for pure convection cases

Fig. 7 shows streamlines and isotherms for $Ra = 10^{12}$ with three different values of AR. The temperature contours are plotted for 20 equally spaced values. For an aspect ratio 0.5, a double cell flow pattern similar to Rayleigh Bénard convection is seen with the plume nearly at the centre of the enclosure. Individual cells are not identical, with the right cell being weaker. When the AR increases, this discrepancy further increases leading to a primary counter clockwise vortex cell with a weak secondary vortex at the top right corner.

Interestingly, it was observed that the location and direction of these vortex cells get exactly interchanged when an initial disturbance is given to the flow field. It may be noted that the grids used in these computations are symmetric in the X-direction. The distribution of convective Nusselt number on the bottom wall for these two different solutions are presented in Fig. 8, for AR = 1 and $Ra = 10^8$. The first solution is obtained with initial conditions corresponding to the rest state (i.e., $u = 0$ and $v = 0$) and leads to an anti-clockwise primary cell. When the solutions are obtained with initial guess values of velocities, steady state solutions are obtained leading to a clockwise rotating primary cell. Both solutions lead to the same

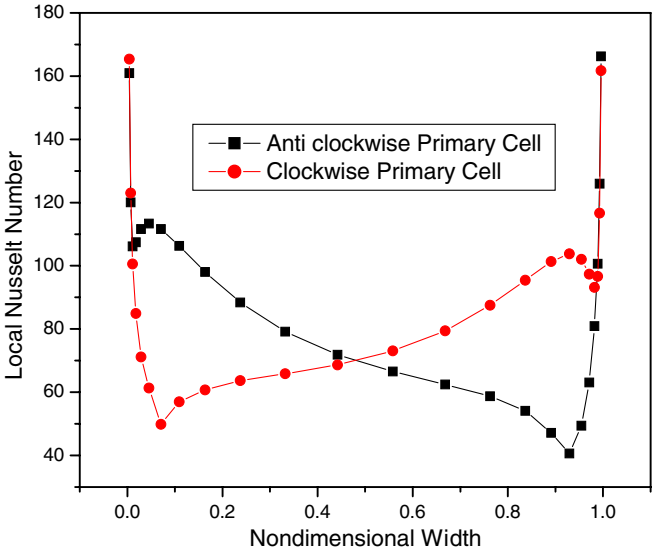

Fig. 8. Distribution of convection Nusselt number on the bottom wall for $Ra = 10^8$ and AR = 1.0.

average Nusselt number values with a marginal loss in symmetry, when one considers the distribution of the local convective Nusselt numbers on the bottom wall. This establishes that for turbulent natural convection in enclosures, depending on the initial disturbance in the enclosure, the flow field will set in any direction and is not symmetric. The flow pattern may also change from monocellular to bicellular. A similar phenomenon in laminar natural convection has been observed by Hasnaoui et al. [2] and Ridouane et al. [17], which investigated laminar natural convection in a square cavity heated from below and cooled from the top.

Fig. 9 depicts stream lines and isotherms for a particular aspect ratio of 1 for various values of *Ra* number. The natural convective velocity in the enclosure is known to scale as $H^{1/2}$ and circulation rate, ψ, scales as velocity $\times H$ or $Ra^{1/2}$. The maximum value of the stream function for various *Ra* values is found to be in good agreement with this scaling. It is clear that at small values of *Ra*, the isotherms fill the enclosure in a relatively uniform way and as *Ra* increases, the isotherms are concentrated close to the walls, leading to a nearly isothermal bulk fluid at the central part of the enclosure. The temperature of the bulk fluid is nearly 0.25 as expected. The average Nusselt number on the

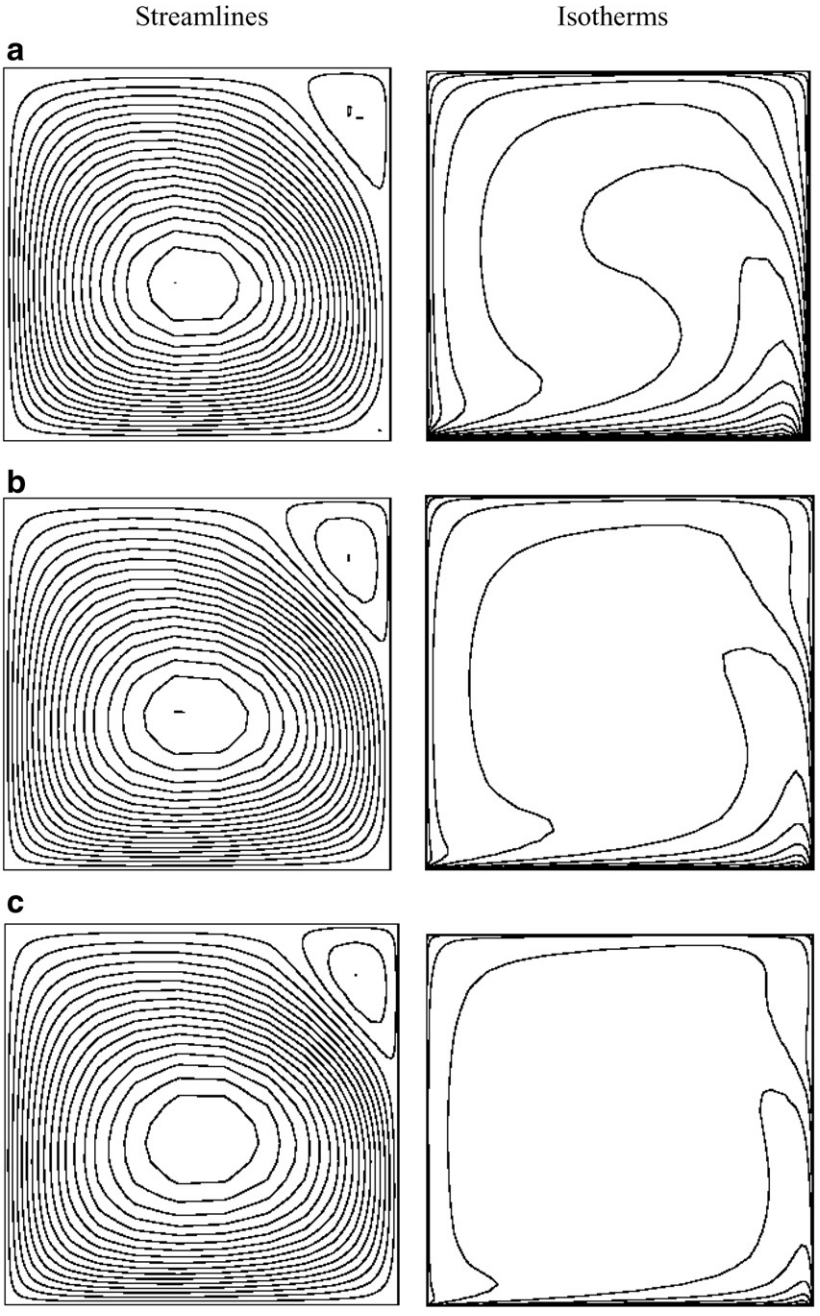

Fig. 9. Streamlines and isotherms: (a) $Ra = 10^8$, $\psi_{max} = 0.011$; (b) $Ra = 10^{10}$, $\psi_{max} = 0.0926$ and (c) $Ra = 10^{12}$, $\psi_{max} = 0.799$ for an enclosure with AR = 1.0.

Table 4
Average Nusselt number on the hot floor for an infinite external heat transfer coefficient in enclosures of different aspect ratios

Rayleigh number	Average Nusselt number			
	AR = 0.5	AR = 1.0	AR = 1.5	AR = 2.0
10^8	71.0	80.4	87.1	98.4
10^9	144.8	166.7	190.7	208.1
10^{10}	308.6	360.7	419.9	449.1
10^{11}	686.8	788.2	955.9	1043.9
10^{12}	1537.1	1820.5	2085.4	2197.3

bottom hot wall for various aspect ratios of the enclosure for $10^8 \leqslant Ra \leqslant 10^{12}$ are given in Table 4. With regard to the variation of the convection Nusselt number (Nu_C) as a function of the aspect ratio AR, when this ratio increases, Nu_C increases. For a low Ra of 10^8, as the aspect ratio increases stratification in the core region is reduced and a marginal increase in the heat transfer occurs with an increase in AR. However, as Ra increases there is quite a sharp increase in the heat transfer rate from the bottom of the enclosure, for a given AR (Table 4). This is because as Ra increases, and consequently the circulation inside the enclosure, the hotter fluid tends to occupy the centre region, compressing the isotherms near the cold walls and near the heated floor.

A correlation has been developed to predict the overall heat transfer rate from the enclosure, for the pure convection cases using multiple linear least square regression and this is

$$Nu_C = 0.152\ \mathrm{AR}^{0.267}\ Ra^{0.34} \tag{11}$$

where Ra is defined based on the enclosure width. Eq. (11) has a correlation coefficient of 99.9% and the standard error on the exponent of Ra is ± 0.002 while the standard error on the exponent 0.267 is ± 0.014. The correlation has an RMS error band of $\pm 3\%$ and is valid for the following range of parameters: $10^8 \leqslant Ra \leqslant 10^{12}$, $0.5 \leqslant \mathrm{AR} \leqslant 2.0$. Alternatively, one may adjust the exponent of Ra to the more commonly used 1/3 and upon doing this, the constant of the correlation (Eq. (11)) becomes 0.177.

4.2. Interaction of natural convection and surface radiation

For finite values of the heat transfer coefficient on the external surfaces of the cold walls, the wall temperature distribution depends on the heat balance among convection/radiation on the internal surfaces, conduction in the walls and convection from the external surfaces. The internal natural convection depends on the wall temperature distribution, thus bringing in, interaction between natural convection and surface radiation. To enable detailed

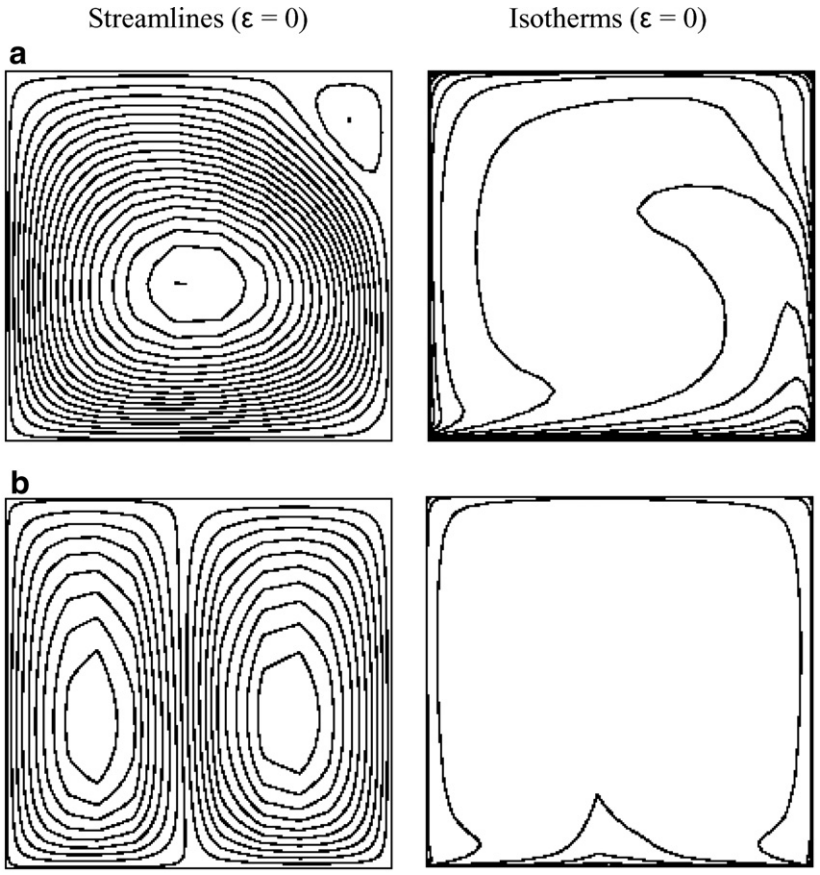

Fig. 10. Streamlines and isotherms: (a) $Ra = 10^8$, $\psi_{max} = 0.00981$ and (b) $Ra = 10^{12}$, $\psi_{max} = 0.340$ for enclosure of AR = 1.0 ($\varepsilon = 0$, $h_{ext} = 5$ W/m^2 K).

understanding, the wall thickness is taken to be negligible to avoid longitudinal heat conduction in walls.

The flow and temperature distribution in the enclosure for a limiting case of zero emissivity at Ra of 10^8 and 10^{12} for unit aspect ratio are presented in Fig. 10a and b, respectively. It can be seen that as a result of finite external convection, the temperature distribution on the cold walls has got modified. This completely changes the flow distribution in the enclosure to a double cell pattern compared to the unicell pattern observed in the case of infinite external heat transfer coefficient (Fig. 9c). Due to an increase in the temperature levels of the cold wall, the magnitude of natural convection velocity has been reduced. This is clear from the reduction in the maximum stream function value from 0.799 to 0.340, as, for example, when $Ra = 10^{12}$.

In order to understand the significance and role of radiation, the emissivity of the walls is set to 0.9. The corresponding flow and temperature distribution are shown in Fig. 11a and b for Ra of 10^8 and 10^{12}, respectively. As a result of surface radiation, the temperature levels of cold wall increase further, which further dampens the natural convection. This is clear from the reduction in the maximum stream function value from 0.340 to 0.314 for $Ra = 10^{12}$. Similar results were also obtained for a Rayleigh number of 10^{11}.

The non-dimensional gas (air) temperature distribution along the mid height of the enclosure and along the mid width of the enclosure is depicted in Fig. 12a and b, respectively, for Rayleigh number 10^{10}. It is clear from these figures that for $\varepsilon = 0$, the overall temperature level of the walls and gas in the enclosure is less than that for $\varepsilon = 0.9$.

Values of convective, radiative and overall mean Nusselt numbers on the hot floor of the square enclosure are presented in Table 5, for various values of Ra. Comparing Tables 4 and 5 for pure natural convection cases of AR = 1.0, it is clear that for a finite external heat transfer coefficient the Nusselt number is only about 60% of the value corresponding to case of an infinite heat transfer coefficient. This is due to an overall reduction in the convective flow, which is a consequence of the reduction in the effective driving temperature difference between the hot and cold walls.

Similarly, on comparing the convective Nusselt number for $\varepsilon = 0$ and $\varepsilon = 0.9$ in Table 5, it is clear that surface radiation reduces natural convection by reducing the effective driving temperature difference leading to a reduction of approximate 25% in the convective Nusselt number. But the contribution of radiation is of similar order as that of natural convection. Interestingly, the total contribution of natural convection and surface radiation is very close to the natural convection contribution with infinite external heat transfer coefficient (Table 4).

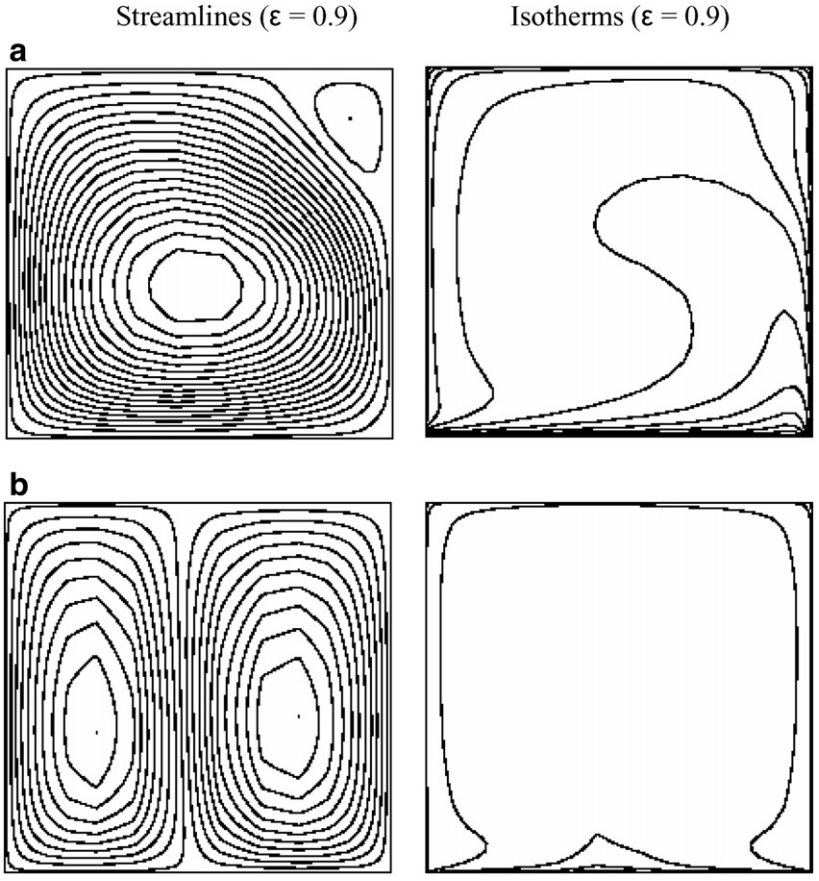

Fig. 11. Streamlines and isotherms: (a) $Ra = 10^8$, $\psi_{max,r} = 0.0085$ and (b) $Ra = 10^{12}$, $\psi_{max,r} = 0.314$ for enclosure of AR = 1.0 ($\varepsilon = 0.9$, $h_{ext} = 5$ W/m^2 K).

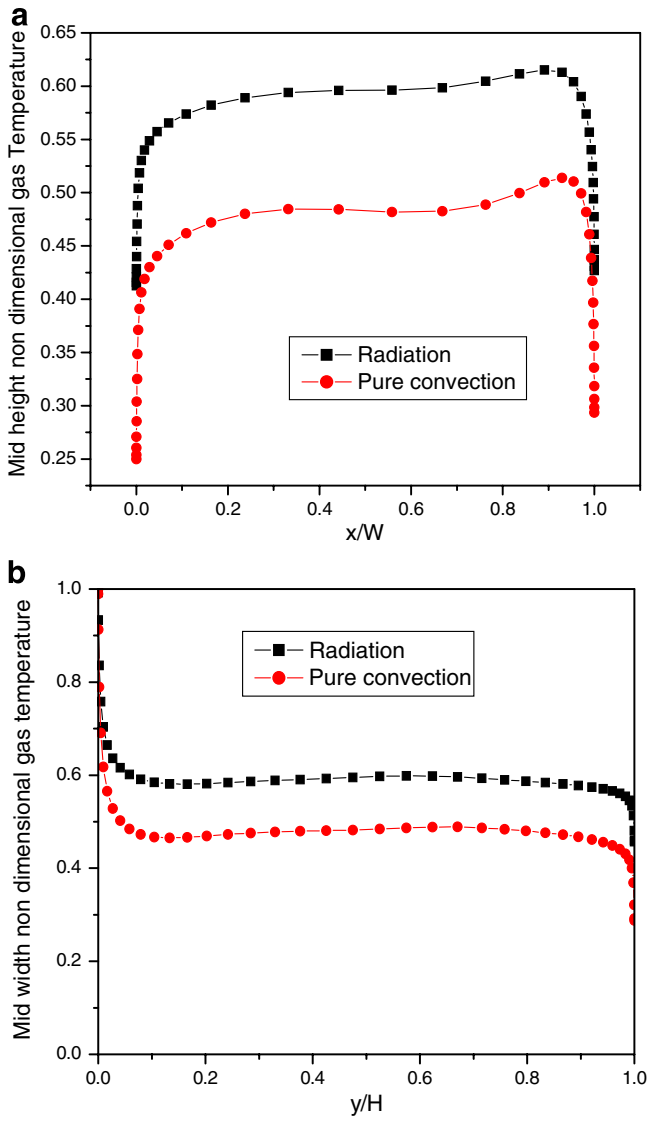

Fig. 12. Variation of gas temperature for $Ra = 10^{10}$ and AR = 1.0 at (a) mid height and (b) mid width.

Table 5
Average Nusselt number on the hot floor for a finite external heat transfer coefficient of 5 W/m^2 K in an enclosure of AR = 1.0

Rayleigh number	Pure convection ($\varepsilon = 0.0$)	Convection with radiation interaction ($\varepsilon = 0.9$)		
	Nu	Nu_R	Nu_C	Nu_T
10^8	47.19	38.51	35.24	73.75
10^9	101.26	83.31	75.83	159.14
10^{10}	219.68	178.86	165.43	344.29
10^{11}	508.19	379.05	387.26	766.31
10^{12}	1174.24	806.25	871.3	1677.55

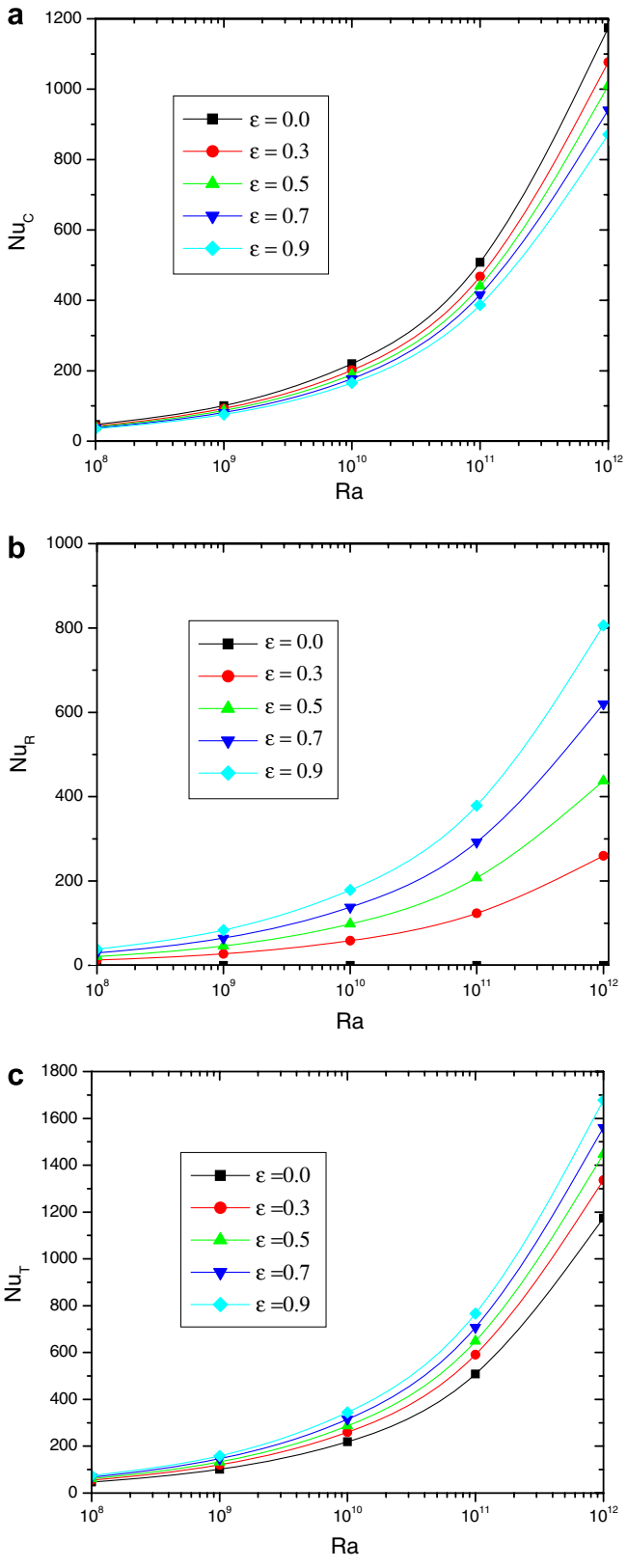

Fig. 13. Variation with Ra of: (a) Nu_C; (b) Nu_R and (c) Nu_T for various values of the emissivity.

4.3. Effect of the wall emissivity on the heat transfer from the enclosure

The effect of wall surface emissivity is analysed for $10^8 \leqslant Ra \leqslant 10^{12}$, for an enclosure of AR = 1.0, with a convective heat transfer of 5 W/m^2 K on the external surfaces of the cold walls. The emissivity value is varied from 0 to 0.9 and the individual contributions of convection and

radiation to the total Nusselt number are presented. Fig. 13(a–c), show the variation of convective Nusselt number (Nu_C), Radiative Nusselt number (Nu_R) and total Nusselt number (Nu_T) with Ra number, for different values of emissivity. Surface radiation is seen to reduce the convective Nusselt number. Larger the value of emissivity, larger is the reduction in convective Nusselt number. This reduction is about 18–27% and the same is compensated well by radiation heat transfer. With an increase in the emissivity, the temperature of the cold walls increases which reduces the driving temperature difference for convection, leading to a reduction in the convective heat transfer. The radiative Nusselt number increases sharply with increase in emissivity. For the high emissivity ($\varepsilon = 0.9$), the radiative Nusselt number becomes nearly equal to the convective part.

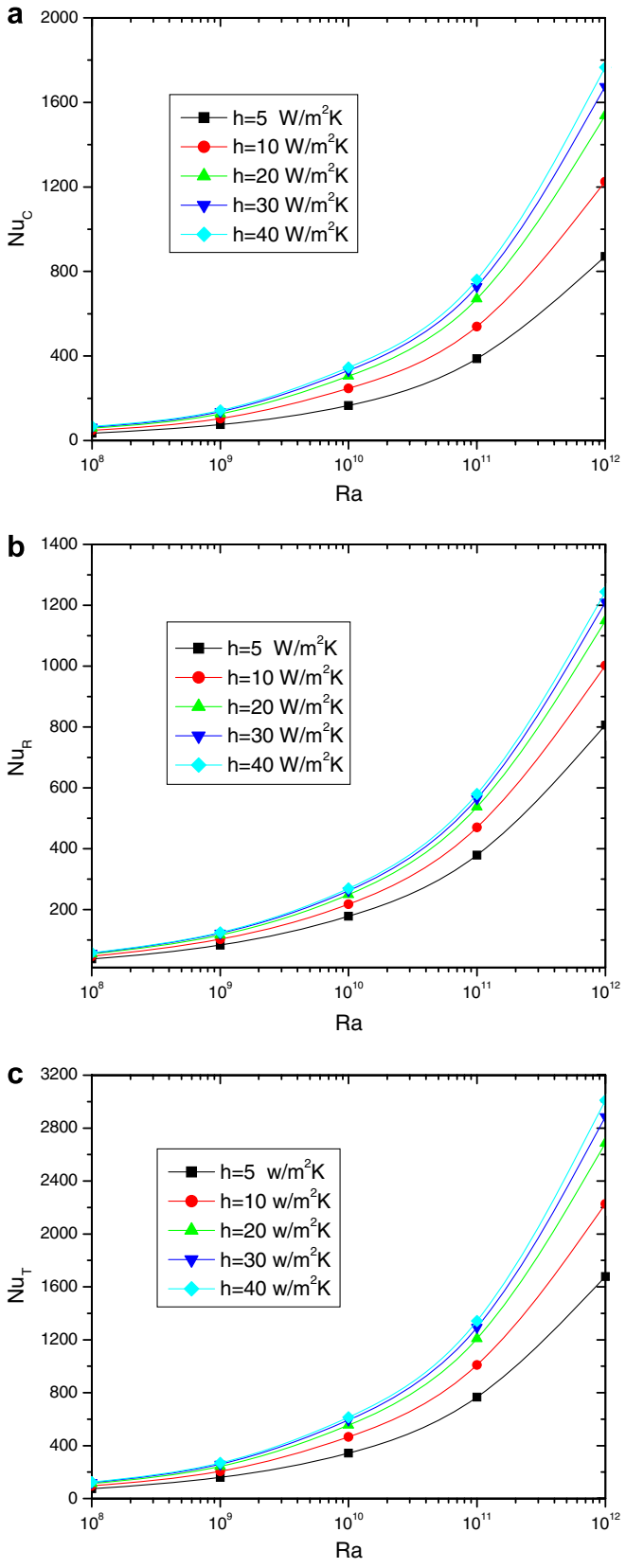

Fig. 14. Variations with Ra of: (a) Nu_C; (b) Nu_R and (c) Nu_T for various convective heat transfer coefficients at outer surfaces of the enclosure.

4.4. Effect of external heat transfer coefficient

The influence of the external heat transfer coefficient (h_{ext}) on the outer surfaces of the cold walls is also studied in detail for a square enclosure. The heat transfer coefficient is varied from 5 to 40 W/m^2 K, which is in the range of heat transfer coefficients obtained for the probable wind velocities existing around the practical enclosures and from the experimental data of Clausing et al. [18]. Fig. 14(a–c), show the dependence of convective, radiative and total Nusselt number on external heat transfer coefficient for various values of Ra. It is seen that as the external heat transfer coefficient increases, the cold wall temperature decreases enhancing the driving temperature differential for natural convection. As a result of these, both the internal convective and radiative Nusselt numbers increase and thereby there is a significant increase in the total Nusselt number. The increase in the convective part is found to be significant compared to that in radiative Nusselt number. For a fixed value of Ra, an increase in 'h_{ext}' by 8 times increases the convective Nusselt by ~90% and radiative Nusselt number by ~50%. Hence the total Nusselt number is increased by about 70%.

5. Conclusions

Turbulent natural convection coupled with surface radiation has been studied numerically in enclosures heated from bottom. The comprehensive 2-D numerical model considers turbulent natural convection of fluid in the enclosure, surface radiation heat transfer among the walls, longitudinal heat conduction in the walls and external convection from the walls simultaneously. Studies have been carried out for a wide range of influencing parameters viz. Rayleigh number, enclosure aspect ratio, emissivity of the wall surface and external heat transfer coefficient. It is seen that the flow distribution in the enclosure is influenced by the external heat transfer coefficient and surface radiation for Rayleigh number $\geqslant 10^{11}$. A unicell flow pattern for aspect ratio $\geqslant 1$, in the case of isothermal cold walls changes to a double cell flow pattern for conducting and radiating enclosure walls. A correlation for the average convection Nusselt number of heated wall is derived in

terms of Rayleigh number and aspect ratio. Surface radiation is found to dampen natural convection and as a result the convective contribution to heat transfer is reduced by ~18–27%. However, this reduction in the convection effect is principally compensated by the contribution of radiation. These results emphasise the need for coupling radiation and convection for accurate prediction of heat transfer in enclosures. The effect of an increase in the external convective heat transfer coefficient on the enclosure walls is more pronounced on the convective heat transfer from the enclosure compared to its effect on radiation.

The enclosures considered in this study represent a simplified geometry compared with the situations usually found in practice. Even so, it provides conditions within which the fundamental mechanisms governing the wall heat transfer and fluid flow under the influence of gravity can be studied. It is therefore hoped that this kind of investigation would lead to an improved knowledge and add to the existing database necessary to (1) evaluate and improve natural convection and radiative cooling capabilities of nuclear reactor subsystems and (2) improve current building design and practice, where saving of energy, thermal comfort, moisture and pollutant transfer, and control of fire and smoke spread are of prime importance.

References

[1] Orhan Aydin, Wen-Jei Yang, Natural convection in enclosures with localized heating from below and symmetrical cooling from sides, Int. J. Numer. Meth. Heat Fluid Flow 10 (5) (2000) 518–529.

[2] M. Hasnaoui, E. Bilgen, P. Vasseur, Natural convection heat transfer in rectangular cavities partially heated from below, J. Thermophys. Heat Transfer 6 (2) (1992) 255–264.

[3] L.E. Hawkines, J.A. Khan, G. Yao, A numerical solution of buoyancy driven flow through small openings between two enclosures, Proc. ASME Meeting HTD 198 (1992) 105–112.

[4] Ulises Lacoa, Antanio Campo, Interaction of natural convection and thermal radiation in square cavities, Heat Technol. 6 (1–2) (1988) 1–11.

[5] C. Balaji, S.P. Venkateshan, Interaction of surface radiation with free convection in a square cavity, Int. J. Heat Fluid Flow 14 (3) (1993) 260–267.

[6] Marcelo M. Ganzarolli, Luiz F. Milanez, Natural convection in rectangular enclosures heated from below and symmetrically cooled from the sides, Int. J. Heat Mass Transfer 38 (6) (1995) 1063–1073.

[7] M. November, M.W. Nansteel, Natural convection in rectangular enclosures heated from below and cooled along one side, Int. J. Heat Mass Transfer 30 (11) (1987) 2433–2440.

[8] B. Calcagni, F. Marsili, M. Paroncini, Natural convective heat transfer in square enclosures heated from below, Appl. Therm. Eng. 25 (2005) 2522–2531.

[9] N.C. Markatos, K.A. Pericleous, Laminar and turbulent natural convection in an enclosed cavity, Int. J. Heat Mass Transfer 27 (1984) 755–772.

[10] R.A.W.M. Henkes, Natural convection boundary layers, Ph.D. thesis, Delft University of Technology, The Netherlands, 1990.

[11] R.A.W.M. Henkes, C.J. Hoogendoorn, Comparison exercise for computations of turbulent natural convection in enclosures, Numer. Heat Transfer, Part-B 28 (1995) 59–78.

[12] E. Bilgen, Natural convection in enclosures with partial partitions, Renew. Energy 26 (2002) 257–270.

[13] S.V. Patankar, D.B. Spalding, A calculation procedure for heat, mass and momentum transfer in three dimensional parabolic flows, Int. J. Heat Mass Transfer 15 (1972) 1787–1806.

[14] R. Siegel, J.R. Howell, Thermal Radiation Heat Transfer, McGraw Hill, New York, 1972.

[15] G. DeVahlDavis, Natural convection of air in a square cavity: A bench mark numerical solution, Int. J. Numer. Meth. Fluids 3 (1983) 249–264.

[16] H.N. Dixit, V. Babu, Simulation of high Rayleigh number natural convection in a square cavity using the lattice Boltzmann method, Int. J. Heat Mass Transfer 49 (2006) 727–739.

[17] E.H. Ridouane, M. Hasnaoui, A. Amahmid, A. Raji, Interaction between natural convection and radiation in a square cavity heated from below, Numer. Heat Transfer, Part-A 45 (2004) 289–311.

[18] A.M. Clausing, J.M. Waldvogel, L.D. Lister, Natural convection from isothermal cubical cavities with a variety of side-facings apertures, ASME J. Heat Transfer 109 (1987) 407–412.

[19] S.M. Elsherbiny, G.D. Raithby, K.G.T. Hollands, Heat transfer by natural convection across vertical and inclined layers, ASME J. Heat Transfer 104 (1982) 96–102.